AGU PUBLICATIONS

JGR

Journal of Geophysical Research: Oceans

RESEARCH ARTICLE

10.1002/2014JC010386

Key Points:
- Surface current is amplified in the summer, while subsurface in winter
- WGC system is getting warmer/saltier and slower
- Seasonal velocity changes are baroclinic, and interannual changes are barotropic

Correspondence to:
T. Rykova,
tatiana.rykova@csiro.au

Citation:
Rykova, T., F. Straneo, and A. S. Bower (2015), Seasonal and interannual variability of the West Greenland Current System in the Labrador Sea in 1993–2008, *J. Geophys. Res. Oceans*, *120*, 1318–1332, doi:10.1002/2014JC010386.

Received 28 SEP 2014
Accepted 13 JAN 2015
Accepted article online 22 JAN 2015
Published online 25 FEB 2015

Seasonal and interannual variability of the West Greenland Current System in the Labrador Sea in 1993–2008

Tatiana Rykova[1,2], Fiammetta Straneo[2], and Amy S. Bower[2]

[1]CSIRO Marine and Atmospheric Research, Hobart, Tasmania, Australia, [2]Woods Hole Oceanographic Institution, Woods Hole, Massachusetts, USA

Abstract The West Greenland Current System (WGCS) transports heat and freshwater into the Labrador Sea, influencing the formation of Labrador Sea Water, a key component of the Atlantic Meridional Overturning Circulation. Notwithstanding its importance, relatively little is known about the structure and transport of this current system and its seasonal and interannual variability. Here we use historical hydrographic data from 1992 to 2008, combined with AVISO satellite altimetry, to diagnose the mean properties as well as seasonal and interannual variability of the boundary current system. We find that while the surface, fresh, cold West Greenland Current is amplified in summer, the subsurface warm, salty Irminger Current has maximum transport in winter, when its waters are also warmer and saltier. Seasonal changes in the total transport are thus mostly due to changes in the baroclinic structure of the current. By contrast, we find a trend toward warmer/saltier waters and a slowdown of the WGCS, within the period studied. The latter is attributed to changes in the barotropic component of the current. Superimposed on this trend, warm and salty anomalies transit through the system in 1997 and 2003 and are associated with a rapid increase in the transport of the boundary current due to changes in the baroclinic component. The boundary current changes precede similar changes in the interior with a 1–2 year lag, indicating that anomalies advected into the region by the boundary current can play an important role in the modulation of convection in the Labrador Sea.

1. Introduction

The Atlantic Meridional Overturning Circulation (AMOC) is a major contributor to the transport and storage of heat, freshwater, and other tracers in the ocean. One of the key components of the AMOC is intermediate water formation in the Labrador Sea. This transformation has been extensively studied over the past few decades and significant progress has been made toward understanding the processes and forcing mechanisms that contribute to the duration and extent of convection in the interior of the Labrador Sea [*Lab Sea Group*, 1998; *Marshall and Schott*, 1999; *Lazier et al*., 2002; *Pickart et al*., 2002]. Similarly, a number of studies have estimated the production rates and the pathways and transformation as the intermediate water spreads from the formation site [e.g., *Rhein et al*., 2002; *Bower et al*., 2009]. Fewer studies, however, have focused on the West Greenland Current System (WGCS), the boundary current system that supplies the Labrador Sea with relatively light waters that are then transformed into Labrador Sea Water (LSW), the dense water produced in the Labrador Sea. Those that have primarily focused on how these light waters are transported into the convection region and, in particular, on a high eddy kinetic energy region where warm buoyant eddies form and advect light waters into the Labrador Sea [e.g., *Prater*, 2002; *Lilly et al*., 2003; *Katsman et al*., 2004; *Bracco et al*., 2008; *de Jong et al*., 2014]. The structure of the inflowing current itself, and its variability on seasonal to interannual time scales, however, are largely unknown—in part because of the lack of long-term measurements here. The work by *Bacon et al*. [2008] summarizes our knowledge about the inflowing waters and their interannual transport variability up to date.

The inflowing boundary current system, west of Greenland, is composed of several components at different depths (Figure 1) [*Cuny et al*., 2002; *Pickart et al*., 2002]. In the top 200 m, the West Greenland Current (WGC) carries cold and freshwaters from the Arctic Ocean and from Greenland freshwater discharge. Beneath the WGC, and to its offshore side, the Irminger Current (IC, 200–1000 m depth range) carries warmer and saltier subtropical waters from the North Atlantic Current into the Labrador Sea. Beneath the IC, this boundary current system carries the intermediate and dense waters formed in the subpolar gyre, including LSW, as well

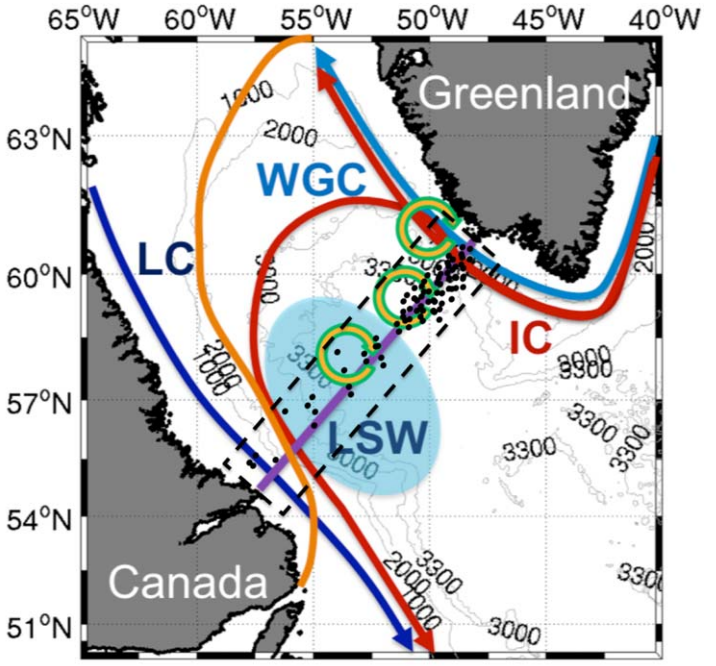

Figure 1. Schematic of the Labrador Sea with the surface currents identified. Light blue region represents interior, purple line is AR7W, the black dots denote the approximate location of profiles used within the 100 km region of AR7W also denoted by the dashed black box, and the yellow circles are the eddies, arrows represent the currents: WGC West Greenland Current (light blue), IC Irminger Current (red); LC Labrador Current (dark blue), the maximum ice extent indicated in orange. Gray contours represent bathymetry: 1000, 2000, 3000, and 3300 m indicated.

as those originating in the Nordic Seas [e.g., *Dickson and Brown*, 1994; *Pickart and Spall*, 2007]. This deeper portion of the boundary current is known as the Deep Western Boundary Current [e.g., *Dickson and Brown*, 1994]. Here we largely focus on the buoyant portion of the inflowing boundary current, i.e., the WGC and IC portions, found inshore of the 3000 m isobath [*Cuny et al*., 2002]. Since we are interested in the source waters for LSW, we here focus on the region southward of 62°N, i.e., upstream of the high eddy kinetic energy region where a significant fraction of the exchange with the interior by eddies takes place.

Data-based studies of the WGCS until now have yield mean reconstructions, based on summer hydrography with velocities referenced to float data [*Pickart and Spall*, 2007], estimates of interannual variations based on changes in single water mass properties [*Myers et al*., 2007], and studies that combines modeling approaches and observations [*Myers et al*., 2009]. Yet, its seasonal variability, or the interannual variability of the entire current (including its transport) are largely undocumented—in part due to the limited amount of data collected here. Understanding this current and its variations, however, is crucial to understanding the process of water mass transformation in the Labrador Sea and how it may be affected by anomalies propagating in from upstream. As shown by *Schmidt and Send* [2007], the WGC is a major source of freshwater for the interior of the Labrador Sea and has the potential to strongly impact the transformation process in the Labrador Sea interior. *Bacon et al*. [2008] documents the WGC transport variability in the multidecadal time series at different locations along the west Greenland coast. This is particularly important in light of the recent changes that have occurred in the Subpolar Gyre (SPG). Since the mid-1990s, the temperature and salinity of the entire SPG, including the Irminger Sea and the Iceland basin, have increased [e.g., *Yashayaev et al*., 2007; *Sarafanov et al*., 2010]. This warming and salinization has been accompanied by a weakening of the SPG circulation observed from altimetry and sparse moored data on the Labrador side [*Häkkinen and Rhines*, 2004; *Hakkinen and Rhines*, 2009] and supported by the modeling studies [*Böning et al*., 2006]. These changes have been largely attributed to the North Atlantic Oscillation (NAO), one of the major modes of atmospheric variability in the Northern Hemisphere, which transitioned from a positive phase to a mostly negative or nonpersistent phase in the mid-1990s [e.g., *Dickson et al*., 2002; *Lazier et al*., 2002]. Yet, the manifestation of these changes in the inflow into the Labrador Sea, and how these may, in turn, have impacted the Labrador Sea interior and the dense water formation here are largely unknown.

Some indication that remotely advected anomalies are important is provided by studies documenting anomalous warming of the Labrador Sea in 1996/1997 and 2003 [e.g., *Brandt et al*., 2004; *Avsic et al*., 2006; *Hakkinen and Rhines*, 2009]. These years were characterized by large lateral heat fluxes between the boundary current and the interior (estimated as the residual of the interior heat content change minus the surface heat flux [e.g., *Brandt et al*., 2004; *Avsic et al*., 2006]) that led to a rapid warming of the central Labrador Sea, affecting the amount and properties of LSW [e.g., *Bersch et al*., 2007; *Yashayaev et al*., 2007].

In at least one of these years, these changes in LSW properties were associated with an increase in the number of eddies reaching the interior of the Labrador Sea [*Lilly et al*., 2003]. The associated increase in lateral heat fluxes, confirmed by an increase in altimeter-derived eddy kinetic energy, led to an anomalous warming of the interior, an increase in the stratification and, eventually, a reduction in the convection [*Lilly et al*., 2003; *Böning et al*., 2006]. None of these studies, however, documented changes in the boundary current flowing into the Labrador Sea and what role they may have played in changes in the lateral heat fluxes.

More recently, studies have begun to address interannual variations in the warm, salty portion of the WGCS [*Stein*, 2005; *Myers et al*., 2007] and its transport [*Myers et al*., 2007, 2009]. These studies, however, have largely focused on summer surveys only and the variability of the current is simply inferred from changes in the top 700 m within the current.

Here we address this gap by investigating both the mean structure of the WGCS, its transport, and its seasonal and interannual variability. Next, we use some simple theory to investigate how this variability may affect the lateral exchange with the Labrador Sea interior and, ultimately, its properties. In section 2, we describe the processing and characteristics of the hydrographic and satellite data and describe how the absolute velocity sections are computed. The mean structure, seasonal and interannual variability of both components of the current are shown in section 3. It is followed by the discussion and conclusions in section 4.

2. Data and Methods

In this section, we describe the in situ hydrographic data and the satellite altimetry products used to obtain the mean properties and absolute velocities of the WGCS.

2.1. Hydrographic Data

We utilized hydrographic sections of the WGCS from three sources: (1) the Bedford Institute of Oceanography (data courtesy of I. Yashayaev), including their annual occupation of the World Ocean Circulation Experiment (WOCE) AR7W section from 1990 to 2004, [e.g., *Yashayaev et al*., 2007]; (2) Hydrobase (www.whoi.edu/science/PO/hydrobase/) [*Curry and Mauritzen*, 2005]; and (3) International Council for the Exploration of the Sea (ICES, Denmark—www.ices.dk) covering the years up to 2006. We restrict ourselves to the data collected after October 1992, when satellite altimetry product became available. Consistent with WOCE standards, the accuracy of the all hydrographic data is 0.002°C for temperature, 0.002 psu for salinity, and 3 dbar for pressure. Most of the sections in the area of interest are aligned with the AR7W line with stations spaced ∼20–55 km in the interior of the Labrador Sea and ∼10–30 km in the WGCS. To construct a climatology of the boundary current, we only consider sections taken within 100 km of the AR7W. Our rationale is that along-flow bathymetry does not change considerably over this distance, especially downstream of AR7W where the majority of the stations were, allowing for averaging along bathymetric contours. Note that the region where the WGCS is known to be highly unstable and produce numerous eddies (roughly 52°W, 62°N) [e.g., *Lilly et al*., 2003] is downstream of our sampling box and therefore excluded from our climatology. Data from all three sources were compiled and quality controlled. Duplicate sections, sections which did not have both temperature and salinity data at the same time/location, and sections with questionable profiles were all excluded. To ensure coverage of most of the WGCS, we only considered sections extending deeper than or equal to 1000 m, starting within 30 km of the coast and extending at least 200 km offshore (i.e., from the 200 to the 3500 m isobaths). A total of 18 sections satisfying the criteria outlined above are used in this study (Figure 1). While most of the cruises occurred during late spring and summer, this data set also includes five fall/winter occupations which allows us to capture part of the seasonal variability (Figure 2) in contrast to the earlier studies which have only focused on the summertime data [e.g., *Stein*, 2005; *Myers et al*., 2007]. The wintertime cruises are described in detail in *Lab Sea Group* [1998] and *Pickart et al*. [2002].

To produce the mean fields of potential temperature, salinity, and potential density, we proceed as follows. First, we identified profiles within the sections that occurred in the large, warm eddies produced by the WGCS instability and described in a number of studies [*Prater*, 2002; *Lilly et al*., 2003; *Katsman et al*., 2004; *de Jong et al*., 2014]. Many of these were already identified in *Rykova et al*. [2009] and the same

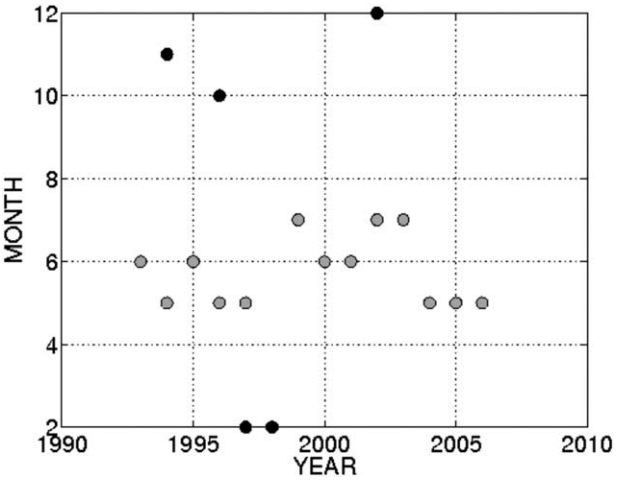

Figure 2. Hydrographic sections occupation, summer (gray) and winter (black).

criteria are used here. Profiles in eddies are those that are 0.1°C warmer and 0.01 psu saltier over a layer that is at least 100 m thick, within the 200–1000 m depth range, and that are separated from the warm water transported by the boundary current by at least one hydrographic station. These profiles are then removed from the section. Second, we interpolate the data onto a regular grid by using the Laplacian-spline interpolation routine following the study by *Fratantoni and Pickart* [2007] and *Våge et al*. [2011]. We interpolate the sections onto a regular grid with 5 km horizontal and 10 m vertical resolution. To extrapolate the data down to the bottom topography, we chose *Smith and Sandwell* [1997] satellite bathymetry to determine the shape of the topographic slope. Finally, sections are projected onto the AR7W line, by moving each station to the corresponding isobath on the AR7W section.

There are two major differences between the climatology presented here and the climatologies from the previous studies [*Stein*, 2005; *Pickart and Spall*, 2007; *Myers et al*., 2007, 2009]. The first is the inclusion of winter and fall data. The second, and more important, is the method for the estimation of the absolute velocity described in detail in section 2.3. In the present work, the relative geostrophic velocity for each of the sections is referenced to the absolute velocity at the surface obtained from AVISO product.

2.2. AVISO Surface Velocity

We use the gridded absolute surface geostrophic velocity from Archiving, Validation, and Interpretation of Satellite Oceanographic (AVISO) website (www.aviso.oceanobs.com) to estimate the surface velocity data along the section. In particular, we use the delayed mode gridded absolute geostrophic velocities that are referenced to the mean state of the current for 1992–2007 (the referencing was provided by the AVISO team). This product is available from October 1992 to January 2008 and consists of a blend from TOPEX-Poseidon, ERS-1, ERS-2, Jason-1, and ENVISAT data interpolated onto a regular 1/3° grid. The use of the gridded product for this study is preferable to using the along-track data for three reasons. First, along-track data often does not coincide with the hydrographic section occupation. Second, the along-track data contains considerable high-frequency variability (daily to weekly), which makes it difficult to reference the hydrographic section to it. Third, along-track products are based on a single satellite and provide less accurate results than the combination of satellites generally used in the gridded data product [*Ablain et al*., 2009]. The gridded absolute surface velocity product is available every 7 days. However, due to the large variability in the boundary current even on daily time scales [*Pickart*, 2013], we choose the gridded mean 28 day averaged maps for further analysis, thus, filtering out most of the mesoscale variability of the boundary current.

Besides the difference in the temporal resolution between the along-track and gridded products, the gridded fields have larger uncertainties. To estimate these, we compared the gridded product with the along-track data in this geographical region. First, since the altimetry product is generally inaccurate along the tracks propagating from land to the ocean on scales on the order of 100 km (L. Traon, personal communication, 2008), we made sure that all the tracks, sampling the boundary current, ascend from the Labrador Sea interior toward Greenland. Then, to evaluate the accuracy of the gridded data product, we compare the gridded SSH with the along-track SSH data product for several arbitrarily chosen dates. We found that the two differ by less than 10%. The largest differences occur at the boundary current front and result from the smoothing of the gridded data product compared to the along-track data. Note that we compare SSH instead of absolute velocity since there is no along-track absolute velocity product. Finally, we compared the gridded and along-track based velocities as follows. We compute velocity from the along-track SSH

data and compare it to the absolute surface velocity from the gridded data product for several arbitrarily chosen times. We found that along-track derived velocity has more variability on small scales and higher velocity (up to twice as large as the gridded product values) at the location of the boundary current front.

Several factors contribute to uncertainties in the absolute velocity estimated from satellite altimetry. These include uncertainties in the satellite performance such as the measurement noise, the wave height contribution, the tidal and orbit errors [*Fu et al*., 1994; *Fu and Cazenave*, 2000]. Another significant error, especially in the coastal areas (closer than 100 km from the shore), is due to the atmospheric forcing. Most of these errors are substantially reduced as a result of the data processing by the AVISO team who compute the atmospheric corrections and minimize the errors via various fitting and filtering (M.-I. Pujol, personal communication and AVISO product documentation, 2010). The pressure and tidal effects are also taken into account during the data processing stage: there are two tidal gauges on the Greenland coast on both sides of AR7W. The merging of the along-track data from different satellites and its gridding is based on the objective analysis that allows producing not only the gridded fields themselves but also the corresponding mapping error fields. The errors originating from the approximations due to the geostrophic balance assumption in calculations of the velocity fields (5–8 cm s^{-1}) are added to the uncertainties mentioned above. The maps of these errors are produced for each gridding and are represented in the percentage of the signal variance that allows us to estimate the relative error as a result of the mapping process. Finally, the gridded product has several weaknesses. The most relevant to this study are: (i) the limited accuracy near the shore (in the boundary current region the product is unreliable shoreward of 30 km from the coast that is roughly equivalent to the 200 m isobath); (ii) low horizontal resolution (1/3°) results in a large uncertainty on the fronts position and width.

2.3. Absolute Velocity From Hydrography and AVISO

We restrict our analysis to the velocity perpendicular to the AR7W section, which is largely perpendicular to the mean topographic slope and is the main component of the flow [*Cuny et al*., 2002]. From the mean property sections, we estimate the geostrophic velocity using the thermal wind relation:

$$\frac{\partial V}{\partial z} = -\frac{g}{f\rho_0}\frac{\partial \rho}{\partial r}, \tag{1}$$

where V is the alongshore velocity, g is gravity, ρ_0 is reference density, f is Coriolis parameter, ρ is potential density, z is vertical coordinate, and r is the distance along AR7W section away from the coast. Integrating this equation in the vertical, we obtain:

$$V(z) = -\frac{g}{f\rho_0}\int \frac{\partial \rho}{\partial r} dz + C(r), \tag{2}$$

where $C(r)$ is a constant of integration, or the absolute velocity at a certain depth.

To obtain an absolute velocity, we reference the relative geostrophic velocity for each of the sections to the surface velocity obtained from the gridded AVISO product. This method is similar to that used by *Han et al*. [2010] who referenced their geostrophic velocities to the along-track satellite product for the Labrador Current, but differs considerably from previous studies of the WGCS that referenced geostrophic velocities to diagnostic model output [*Myers et al*., 2007, 2009], to the mean velocity from the float data for 1994–1999 [*Pickart and Spall*, 2007] or lowered Acoustic Doppler Current Profiler (ADCP) data [*Hall et al*., 2013].

To obtain the velocity in the regions shallower than 1000 m, we used the method described in *Helland-Hansen* [1934], who suggested extending the isopycnals horizontally into the ground. In this case, the isopycnals below the bottom are parallel to each other resulting in zero velocity. The advantage of this method is in the continuous velocity field near the bottom that matters both for the velocity field itself and for the transport calculations.

The resolution of the hydrographic sections (5–10 km) is much finer than the resolution of the AVISO product (30 km) so in order to reference the former to the latter we smooth the hydrographic sections to match the AVISO resolution. Similarly, since it takes several days to complete a hydrographic section and since there is a lot of daily to weekly variability in the region [*Pickart et al*., 2002], we use 28 day mean AVISO for referencing hydrographic sections. A smoothed hydrography matches 4 week mean AVISO perfectly. Following this procedure, the absolute geostrophic velocity for each section is:

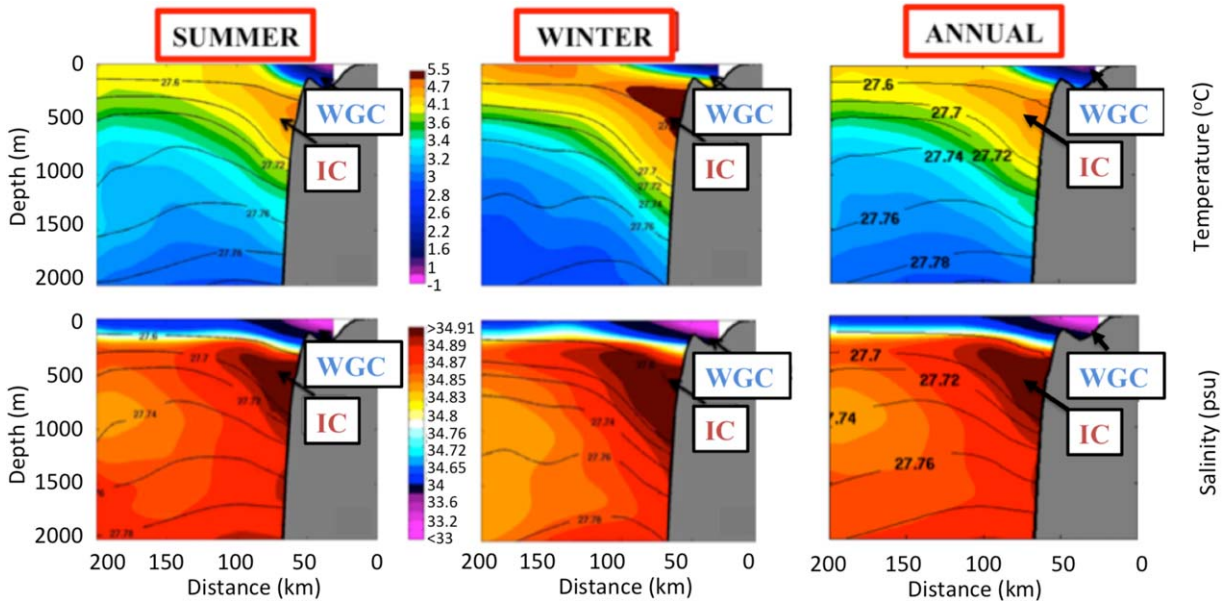

Figure 3. (top) Mean potential temperature and (bottom) salinity sections across the West Greenland Current System for (left) summer, (middle) winter, and (right) annual (see text for description).

$$V(r,z)=V_{AVISO}(r)-\frac{g}{f\rho_0}\int_0^z \rho_r dz, \tag{3}$$

The validity of this method is assessed by comparing with existing synoptic and climatological estimates as well as individual Lowered ADCP velocity data (described in *Hall et al*. [2013] and *Rykova* [2010]). AVISO-derived velocity agrees well with direct measurements (with RMS differences of 2–8 cm s^{-1}), although the ADCP-derived velocity has smaller-scale variability, with amplitudes of up to 0.05 m s^{-1} on scales not resolved by the hydrography.

3. Results

In this section, we first present the annual and seasonal mean sections of temperature, salinity, and surface velocity. Then, we describe the absolute velocity sections and discuss the corresponding transport estimates. Finally, we describe the interannual variability.

3.1. Annual and Seasonal Mean Properties From Hydrography

To investigate seasonal changes, we define a summer season (May to July) and a winter season (October to February), in agreement with the seasonal evolution for the Labrador Sea, where maximum depth of convection is typically observed in April [e.g., *Lilly et al*., 2003; *Straneo*, 2006a]. There are 13 sections in the summer cluster (6 in May, 4 in June, and 3 in July) and 5 in the winter cluster (1 in October, 1 in November, 1 in December, and 2 in February, see Figure 2). Seasonal mean cross sections of potential temperature and salinity for the period 1993–2006 are obtained by averaging sections within the summer and winter clusters (Figure 3). To avoid biasing, the annual mean to the summer period when more sections are available, the annual mean is estimated as the average of the summer and winter means (Figure 3). Although there are only five occupations of the AR7W section during the fall/winter, they cover the mid-1990s (1993 onward), with just one wintertime section in the 2000s. We assume these surveys to provide a representative estimate of the full period.

The major characteristics of the boundary current system are visible in all three sections. Cold, fresh Polar Water (PW) from the Arctic, the main component of the WGC, lies above and onshore of the warmer and saltier Irminger Water (IW), originating from the subtropical Atlantic and transported by the IC from the eastern side of Greenland. In the interior of the Labrador Sea, LSW occupies the 500–1500 m depth range. The dense waters from the Nordic Seas are found beneath LSW in the Deep Western Boundary Current

Table 1. Summer, Winter, and Annual Mean Properties of the IC Core

	Summer	Winter	Annual
Potential temperature (°C)	4.35 ± 0.47	5.00 ± 0.34	4.78 ± 0.28
Salinity (psu)	34.90 ± 0.03	34.91 ± 0.03	34.91 ± 0.03
Potential density (kg m^{-3})	27.67 ± 0.04	27.60 ± 0.03	27.64 ± 0.04

[*Pickart and Spall*, 2007]. In summer, the layer of PW is thicker and fresher at the expense of a thinner, less salty layer of underlying IW. In winter, the situation reverses with a thinner PW and a thicker, warmer and saltier IW. In general, we find that the variability of the WGCS properties, characterized here by the standard deviation, is the largest at the surface where the seasonal cycle is the strongest.

Most of the sections used in this study do not extend far enough inshore to capture the full extent of the shallow, fresh portion of the WGCS. Therefore, we focus primarily on the IC. To compare the IC properties seasonally and interannually, given that the IC is not fully resolved in each individual section, we consider mean changes over the IC core—defined here as the region (area), common to all the sections, centered at depth of 500 m (extending from 300 to 700 m) and distance of 75 km offshore (extending from 65 to 85 km). The upper boundary is set to 300 m to exclude the WGCS fresh component. The lower boundary is set to 700 m to account for seasonally and interannually varying core temperatures. Using this definition, we find that the properties of the IC core are characterized by potential temperature of 4.78 ± 0.3°C, salinity of 34.91 ± 0.02 psu, and potential density of 27.64 ± 0.02 kg m^{-3} (Table 1). A comparison of the core properties in winter and summer shows that the core of the IC is roughly 0.6°C warmer and 0.01 psu saltier in winter and given the error bar, the seasons are statistically different.

3.2. Annual and Seasonal Mean Surface Velocity Properties From AVISO

The time-mean surface geostrophic velocity derived from the AVISO gridded product has a maximum of 30 ± 4 cm s^{-1} (where the error is estimated as the standard deviation from the mean) located about 50 km from the shore (Figure 4). Velocity decreases rapidly toward the coast and less rapidly toward the interior of the Labrador Sea. The maximum velocity in the weekly gridded data can reach up to 60 cm s^{-1}. The error of the mean velocity—based on the signal variance—is 5 cm s^{-1} for most of the section, but up to 8 cm s^{-1} at the peak of the WGCS. The width of the current, defined here as the distance between the coast and the location where the mean northward flow is zero, is about 150 km. This estimate is consistent with studies of surface drifters by *Cuny et al*. [2002]. The mean AVISO-derived surface velocity from the whole AVISO data set compares favorably with the mean surface velocity obtained by averaging AVISO surface velocity during the 18 different weeks corresponding to the hydrographic sections occupation (Figure 4) suggesting that a 18 section mean is a good representation of the full-record mean.

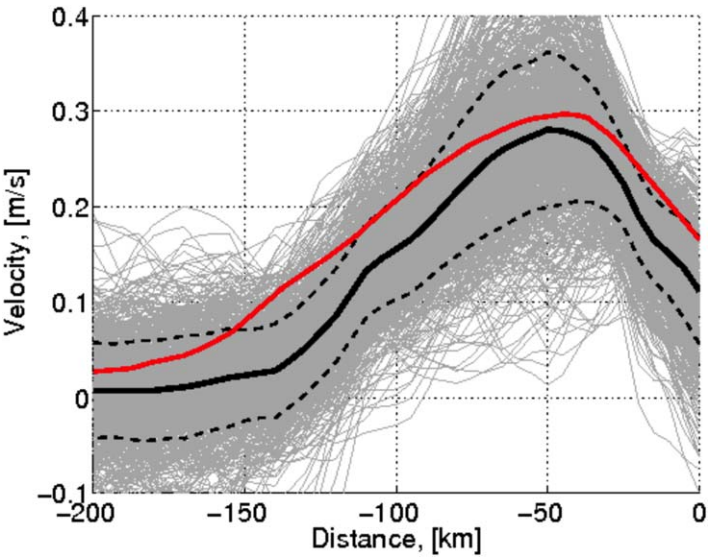

Figure 4. Weekly surface geostrophic velocity, derived from AVISO along the AR7W line from October 1992 to January 2008 (gray lines). Overlaid is the time-mean (black thick line; dashed lines show one standard deviation). The mean surface geostrophic velocity obtained by averaging AVISO surface velocity for the time corresponding to the occupation of the 18 hydrographic sections is overlaid in red, note that this has been smoothed onto the same grid as used for the hydrographic data gridding.

We use the AVISO product to investigate the seasonal variations in the surface currents. To retain the full seasonal variability, we first consider conventional seasons: January through March (JFM), April through June (AMJ), July through September (JAS), and October through December (OND). Both the maximum velocity and currents width at the surface vary seasonally. The

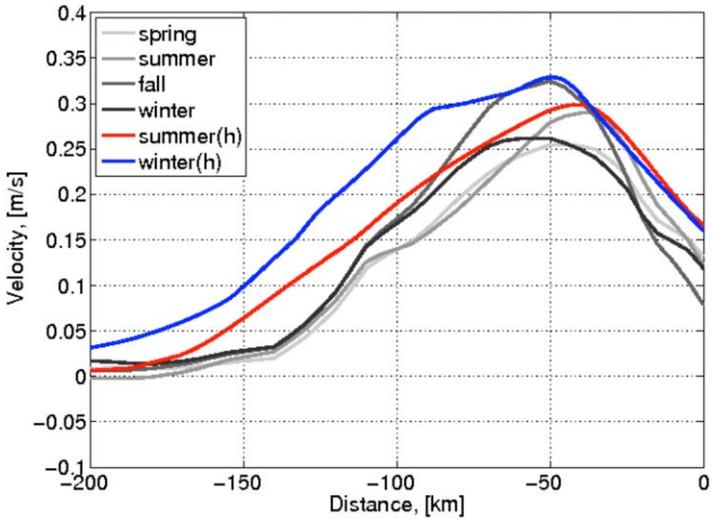

Figure 5. Geostrophic surface velocity derived from AVISO for spring (AMJ, lightest gray), summer (JAS, darker gray), fall (OND, the darkest gray), and winter (JFM, black) as a function of distance from the coast. Overlaid is the summer (May to July) mean (red) and winter (October to February) mean (blue) absolute surface velocity obtained by referencing the geostrophic velocity from the hydrographic sections with AVISO data (see method in section 2.3).

largest velocities occur during the fall (OND) when the current is the widest and the maximum is located approximately 50 km offshore. After that the maximum moves onshore and the velocities become weaker to be minimum during spring (AMJ) (Figure 5).

3.3. Absolute Velocity

To estimate absolute velocities across the section for summer, winter, and the annual mean, we combine hydrography and AVISO, following the method described in section 2.3.

3.3.1. Annual Mean and Seasonal Variability

The absolute velocity section (Figure 6), obtained by referencing the geostrophic velocity derived from the hydrographic data to the AVISO surface velocities (see section 2.3), reveals the full two-dimensional nature of the current system. The interior region is mostly quiescent with a strong, surface intensified flow along the coast of Greenland. Velocities are on the order of 30–35 cm s^{-1} at the surface and decay to a minimum of 3–6 cm s^{-1} below 1000 m. At the depth of the IC core, the mean velocity is 10–20 cm s^{-1} consistent with a previous estimate based on float data *Lavender et al.* [2002]. The offshore portion of the current is remarkably barotropic, consistent with the summer climatology of *Pickart and Spall* [2007] and the individual sections of *Hall et al.* [2013]. Consistent with altimetry and the hydrographic sections, the velocities throughout the water column in the summer mean are weaker than those in the winter mean.

3.3.2. Barotropic and Baroclinic Velocity Components

To investigate whether the winter acceleration of the current is due to the changes in the density structure (baroclinic) or the acceleration of the entire current (barotropic), we decompose the velocity field into a baroclinic and barotropic components. We define the barotropic component as the absolute velocity at 1000 m depth. Accordingly, the baroclinic component is estimated as a difference between the absolute and barotropic velocities (Figure 7). We choose 1000 m since hydrographic data (our own, as well as those discussed by *Pickart and Spall* [2007] and *Yashayaev et al.* [2007]) show that the horizontal density gradients are smallest at this depth—since this is where LSW is present both in the interior and in the boundary

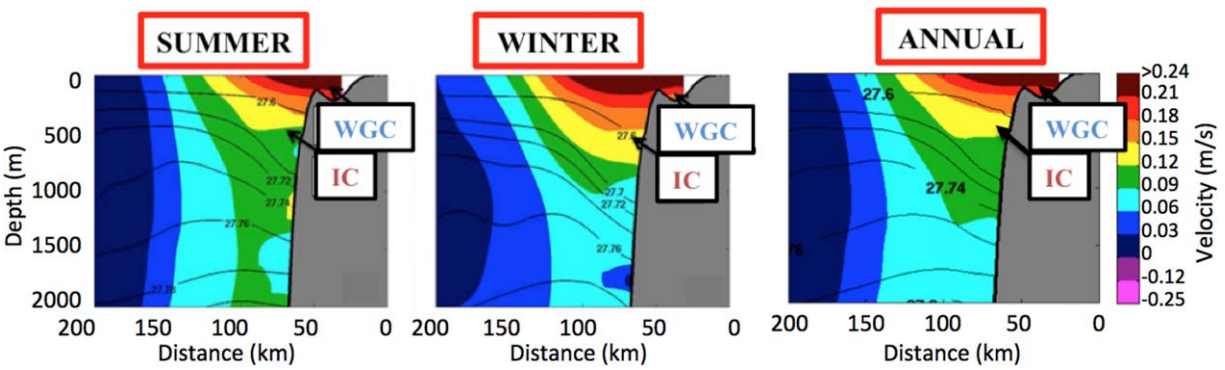

Figure 6. Absolute velocity, with isopycnals overlaid as black contours, in (left) summer, (middle) winter, and (right) annually across the West Greenland Current System.

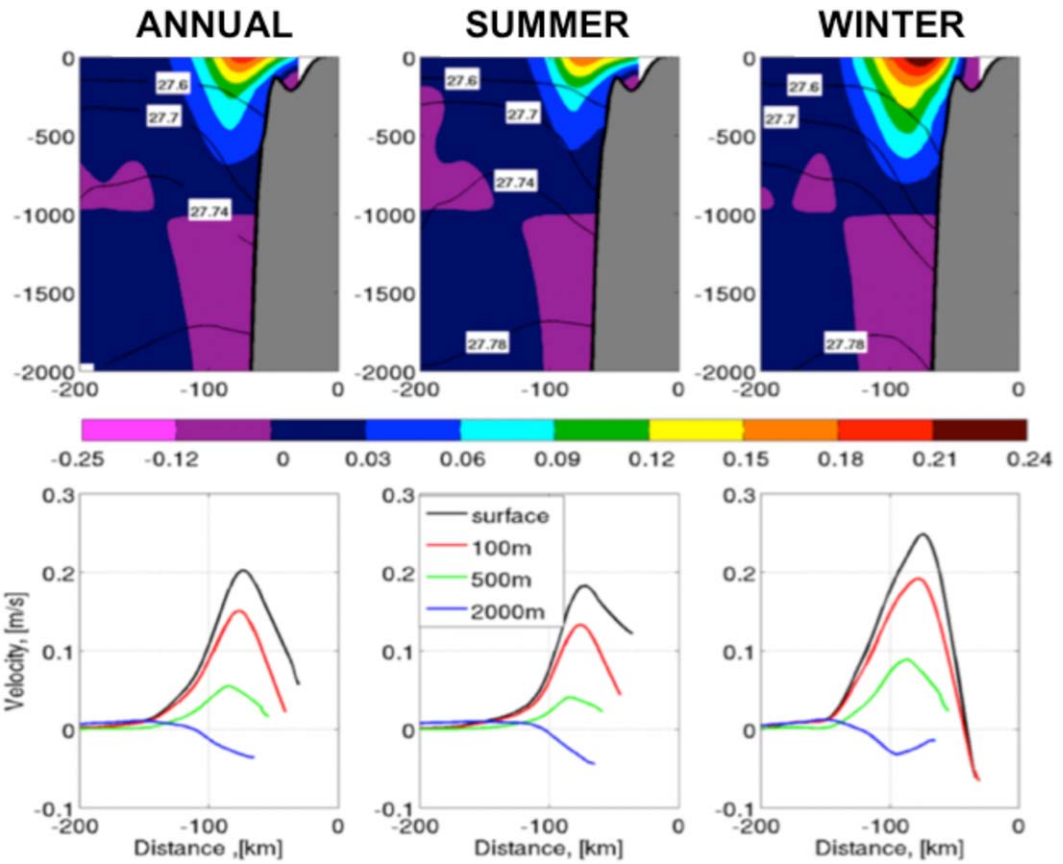

Figure 7. (top) Geostrophic velocity section averaged (left) annually, (middle) summer, and (right) winter; and (bottom) geostrophic velocity at different depths for each time period.

current. Thus, we expect the vertical shear in the mean flow to be small at this depth, making a depth of 1000 m a good choice for a reference level that separates the surface intensified baroclinic component from the barotropic component.

This decomposition reveals that the bulk of the seasonal difference is due to the baroclinic component, as a result of a stronger IC core (Figure 7). Seasonal changes in the barotropic component of the flow are relatively small. Note that the inshore portion of the barotropic flow is not fully resolved due to the fact that 1000 m isobath crosses the section at roughly 65 km offshore (not shown).

3.4. Transport

The total volume transport of the boundary current section that horizontally spans from 0 to 150 km and extends from the surface to the bottom (not shown) is equal to 29.1 $\pm$ 4.8 Sv. This value compares well with the 28.5 Sv estimated by *Pickart and Spall* [2007] from hydrography referenced to the velocity measured by PALACE floats in 1995–1999 [*Lavender et al.*, 2002]. Our mean section also compares favorably with the synoptic velocity sections derived using lowered ADCP data [*Hall et al.*, 2013]. The total transport does not significantly change with season due to compensating changes. In winter, when the upper part of the boundary current (0–2000 m) accelerates, the deeper part of the current (2000 m–bottom) decelerates (not shown).

In terms of the WGC and IC contributions, a comparison with previous estimates is complicated by the nonunique definition of these branches. Here we define the upper portion of the boundary current system that encompasses the WGC and the IC to be that inshore of the 3000 m isobaths (roughly 150 km offshore) and above 1000 m. The 34.4 psu isohaline is chosen as the optimal way of separating the two currents. After considering different definitions based on temperature and salinity gradients, velocity, and potential vorticity, we believe this is the most appropriate choice. For reference, earlier studies used properties to define the IW core (e.g., *Myers et al.* [2007] defined the Irminger Current as the water with $\theta > 3.5^{\circ}$C and S $>$ 34.88 psu) but

Table 2. Volume (T), Heat (HT), and Freshwater Transports (FWT) of the WGC and IC

	T (Sv)			
	WGC	IC	WGC FWT (mSv)	IC HT (TW)
Annual	1.8 ± 0.15	8.1 ± 0.9	60.1 ± 16	153.4 ± 53
Summer	2.0 ± 0.17	7.5 ± 1.1	56.4 ± 19	102 ± 54
Winter	1.7 ± 0.18	8.8 ± 1.6	50.2 ± 17	169 ± 52

we found that these were ill-suited to take into account interannual variations. A more stringent definition of the IW $\theta \approx 4.5^{\circ}$C was used by *Cuny et al.* [2002] but it cuts off the deeper portion of the Irminger Current. The transport estimates using the definition described above are presented in Table 2.

The annual volume transport of the WGC is 1.8 ± 0.15 Sv. Consistent with the widening and deepening of the fresh portion of the current, the WGC transport estimate is larger by about 16% in the summer than in the winter. The summertime freshwater transport referenced to a salinity of 34.3 psu isohaline is 60.1 ± 15.8 mSv, consistent with earlier studies by *Myers et al.* [2009]. The freshwater is mainly brought into the region in summer, likely reflecting a seasonal contribution from melting of sea-ice and glacial melting advected down the east Greenland coast.

The annual IC volume transport is 8.1 ± 0.9 Sv, consistent with the estimates of *Holliday et al.* [2009] upstream. It decreases by roughly 17% in summer consistent with the estimated lower velocities and the decreased extent (Figure 7). The IC is the main contributor to heat advection into the basin, while its freshwater contribution is negligible. The heat transport variability within the IC is larger because the IC velocity is less and the temperatures are colder during the summer. The larger winter volume transport, and the higher IW temperatures and salinities, result in a greater heat transport during the winter (153.4 ± 53.1 TW). While in the winter the volume transport increases only by 17% compared to the summer one, the heat transport increases by as much as 30%. These estimates indicate that the heat transport variability is equally influenced by changes in temperature and velocity of the current.

3.5. Interannual Variability

3.5.1. AVISO

We examine the interannual variability of the surface velocity by computing the monthly mean surface velocities, obtained from AVISO, averaged over the width of the current core (25–75 km offshore; Figure 8). Both summer and winter (not shown) data show a decrease in velocity from 1994 to 2005 of roughly 5 cm s^{-1} over this record, consistent with the decline of the SPG, described by *Häkkinen and Rhines* [2004]. The decrease in velocity may have reversed after 2004. The reader should note that the interannual decrease in velocity is comparable to the characteristic amplitude of the seasonal variability (4–8 cm s^{-1}). There is also a significant year-to-year variability superimposed on this trend, and, in particular, 1997 and 2003 are characterized by large positive anomalies (while 1996 and 2000 are the years with negative anomalies).

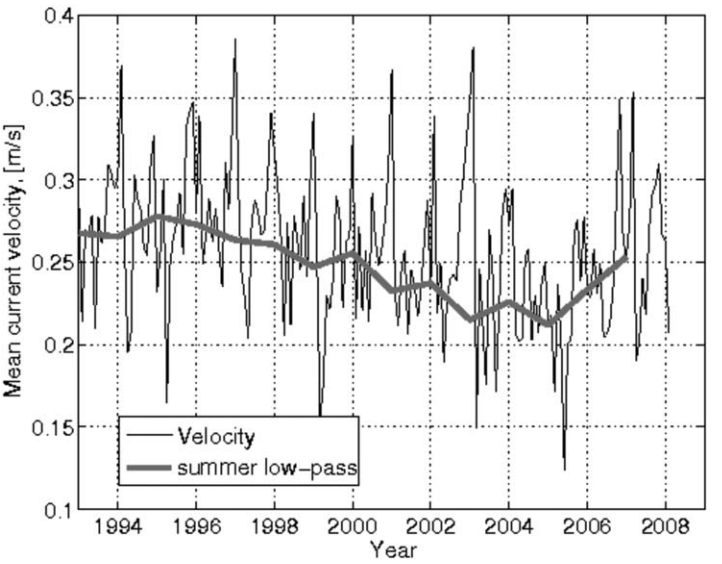

Figure 8. Monthly mean horizontally averaged (25–75 km) surface geostrophic velocity (thin black line) and low-pass filtered summer (JAS) (bold gray line) from AVISO.

3.6. Hydrography

Next, we use hydrography to investigate how the interannual changes in the surface velocity are related to changes of the boundary current at depth. Because we have more summer data, we limit our analysis to the summer hydrographic sections only. The 13 summertime sections are grouped into sections occupied in 1993–1996 and post-1996. This year is associated with a rapid transition of the subpolar gyre to warmer,

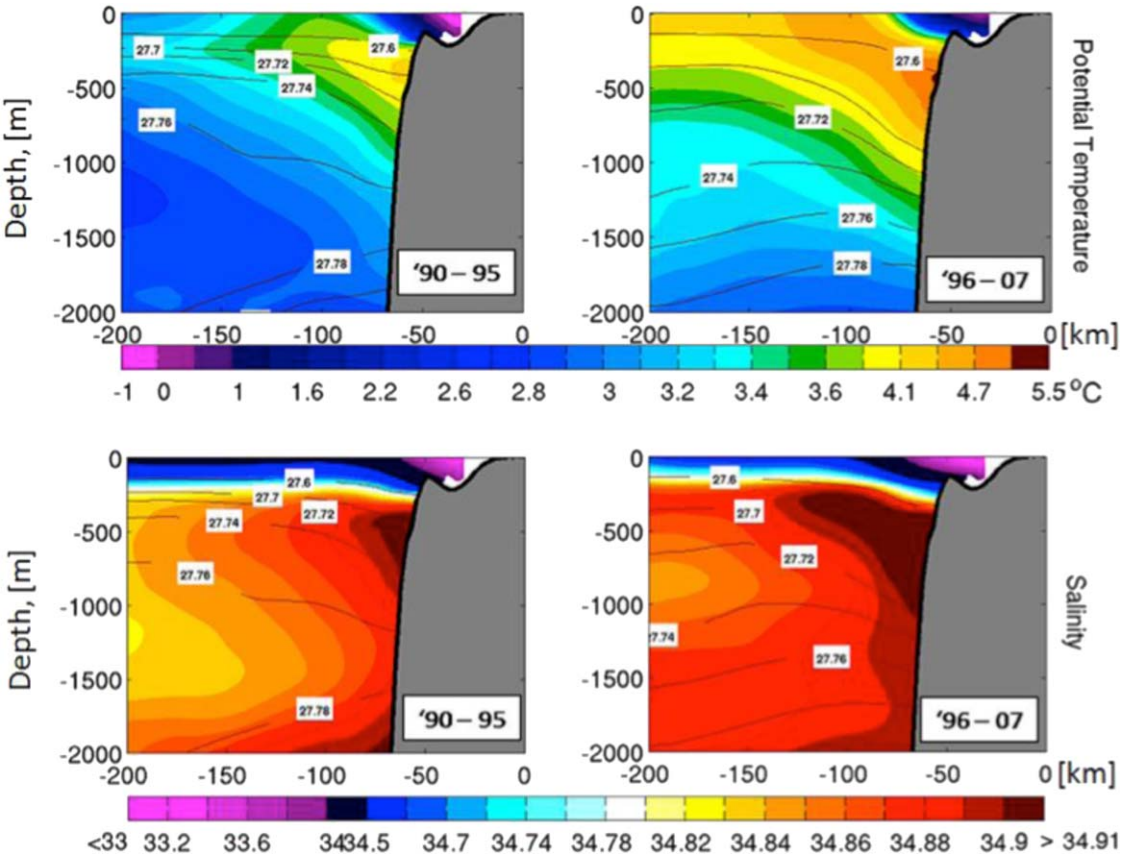

Figure 9. (top) Potential temperature and (bottom) salinity across the West Greenland Current system in summer (left) 1990–1995 average and (right) 1996–2007 average.

slower conditions [*Hátún et al*., 2005; *Hakkinen and Rhines*, 2009; *Våge et al*., 2011]. We show that IW becomes warmer, saltier, and lighter after 1996 (Figure 9), consistent with the model/data-based findings of *Myers et al*. [2007, 2009]. As has been observed on the southeastern side of Greenland [*Våge et al*., 2011], we find that past the mid-1990s the Irminger Current extends farther offshore and is deeper. Due the lack of AVISO product prior to 1993, a reconstruction of the absolute velocity field pre-1996 is impractical (there are only two sections)—thus, we are unable to estimate the transport change associated with the hydrographic property change.

Both our results and previous studies indicate that both the boundary current and the interior of the Labrador Sea warmed from the early 1990s to the 2000s. To investigate the relative change, we compare the IC conditions in the current with those offshore by comparing properties within two boxes in the section. The inshore box, i.e., the "core" of the IC, and the offshore box, the "edge" defined by a rectangle centered at 500 m depth and 150 km offshore (Figure 10d), representing largely the interior properties. Both boxes are 400 m thick and 20 km wide. The inshore/offshore gradient provides a measure of the property differences across the boundary current and hence a measure of the baroclinicity of the boundary current which, in turn, is believed to affect the production of eddies and hence, the heat/freshwater fluxes from the boundary current to the interior [*Spall*, 2004; *Straneo*, 2006b].

Our analysis indicates that comparable warming, salinity increase, and decrease in density trends occur in the inshore and offshore regions, such that overall, the interior/boundary current gradient remains approximately constant (Figures 10a–10c). Superimposed on these trends, 1997 and 2003 stand out as years of significant anomalies in the boundary current which are not observed in the interior. Hence, during both years, the interior-boundary current temperature and density gradients were anomalously large. Interior temperature (density) had a maximum (minimum) 2 years after these anomalies in the boundary current—suggesting a 2 year lag in the propagation of anomalies. These interior anomalies for 1997–1999 and 2003–

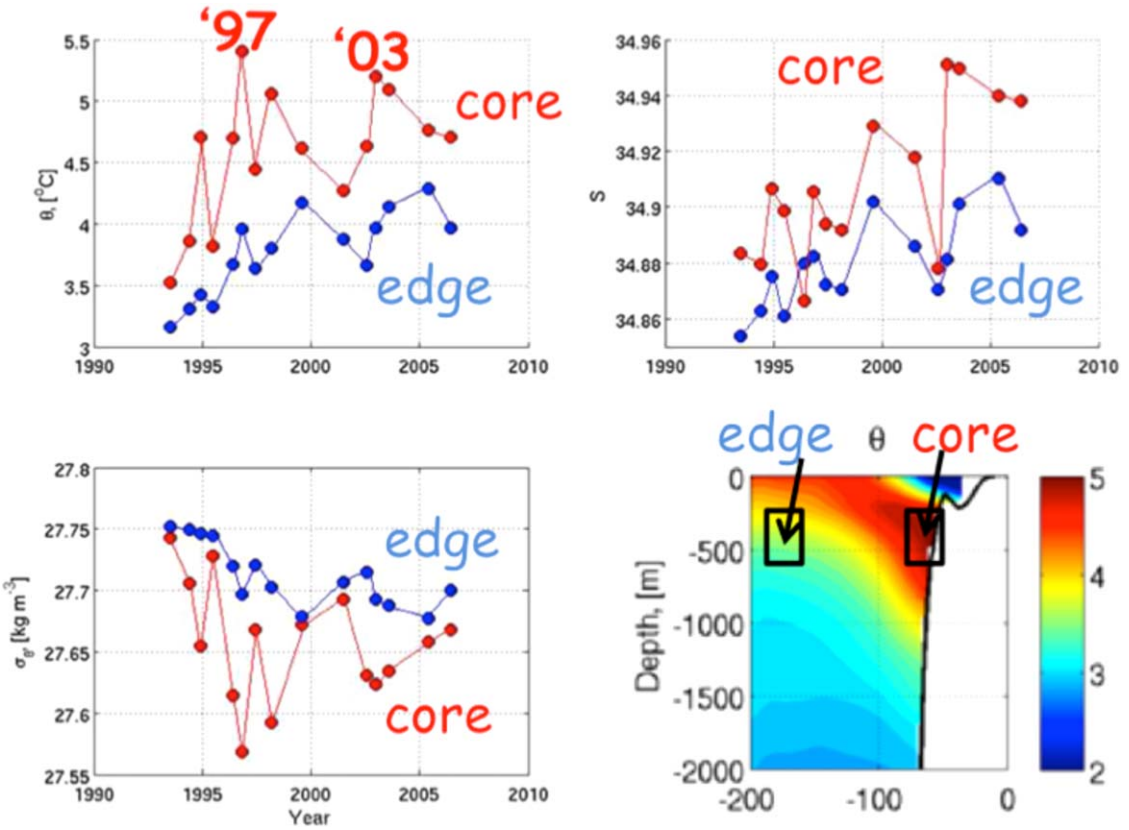

Figure 10. Time series of (a) potential temperature, (b) salinity, (c) potential density for the inner (core, red) and outer (edge, blue) parts of the IC, and (d) schematic of the boundary current.

2005 have also been observed by *Avsic et al*. [2006]. Salinity changes are generally noisier (Figure 10b). The two anomalous years for the boundary current core (1996 and 2003) are characterized by a reversal in the salinity gradient between the inshore and offshore boxes, due to a thickening of the fresh layer during both years which results in a deeper WGC/IC interface. In general, the potential density change in both the core and the edge boxes is dominated by the changes in temperature (Figures 10a and 10c). The implications of these changes are discussed below.

Next, we examine possible changes that the WGC and IC exhibit in the context of recent changes occurring in the SPG. Specifically, the temperature and salinity of the entire SPG have increased since mid-1990s [*Hátún et al*., 2005; *Yashayaev et al*., 2007], while its circulation has decreased [*Hakkinen and Rhines*, 2009]. These changes of the SPG have been partially attributed to the NAO, which transitioned from a positive phase to a nonpersistent phase in the mid-1990s [*Hurrell et al*., 2001; *Dickson et al*., 2002; *Lazier et al*., 2002] but also to changes in the atmospheric blocking between Greenland and western Europe [*Häkkinen et al*., 2011]. The impact of the SPG changes on the properties and transport of the boundary currents around the SPG, however, is not well documented. For example, no trend has been observed in the transport of the East Greenland Current (EGC) from 1992 to 2009 [*Daniault et al*., 2011], while the circulation in the Irminger Sea has intensified [*Våge et al*., 2011]. West of Greenland, there are indications that the salinity of the IC has increased since 1995 [*Myers et al*., 2007] and its transport decreased [*Myers et al*., 2009] based on a combination of sparse hydrographic data and numerical simulations. But there has been no systematic description of the WGCS changes from data.

In particular, beyond the general trends in speed (decreasing) and temperature (warming) from the mid-1990s to present day, there are a few years that stand out as years of rapid change such as 1996/1997 and 2003 [e.g., *Avsic et al*., 2006; *Hakkinen and Rhines*, 2009]. Since lateral fluxes play an important role in the restratification [*Straneo*, 2006b], it is likely that the rapid warming of the central Labrador Sea was related to a large lateral heat inflow from the boundary current. A potentially related change was observed in the

properties and frequency of the Irminger Current Anticyclones (ICAs), the product of the Irminger Current instability, which became warmer, saltier, deeper and increased in numbers after 1997 [*Lilly et al*., 2003; *Rykova et al*., 2009]. The links between the boundary current changes and the interior and eddies' changes are largely unclear.

4. Discussion and Conclusion

The results presented in this study indicate that the properties and velocity of the West Greenland boundary current system, as it enters the Labrador Sea, vary on seasonal to interannual time scales. We show that the warm, salty portion of the boundary current, the IC, is intensified in winter (higher temperature, salinity, and velocity) while the surface portion of the current, the WGC, is faster, thicker, colder, and fresher in the summer. These changes are consistent with those reconstructed from temperature profiles collected by tagged marine mammals along the southeast Greenland shelf [*Straneo et al*., 2010] and with the increase in freshwater transport into the interior documented by *Schmidt and Send* [2007]. Likely, both the freshwater and IC changes are tied to a seasonality in the source waters. For freshwater, this may be associated with a maximum in the volume flux of the East Greenland Current in Fram Strait in March [*de Steur et al*., 2009] or the maximum in sea-ice export in winter/spring [*Kwok*, 2004]. The seasonality in the IC is less obvious. Transport measurements across the IC in southeast Greenland indicate that the transport is maximum in winter [*Daniault et al*., 2011] but the authors do not discuss the seasonal changes in properties.

Our analysis indicates that the isopycnal slope across the IC portion of the WGCS is larger in winter, consistent with the inferred larger instability of the current in winter as documented by the increase in eddy shedding in January–March [*Prater*, 2002; *Lilly et al*., 2003]. This is consistent with the IC being most unstable in the winter (S. Legg, personal communication, 2009), and with the eddy generation being at least partially associated with baroclinic instability. The section in this study is upstream of the eddy generation location so the largest density gradient that we observe in the winter can possibly explain the generation of the eddies downstream. One should keep in mind that our winter season includes the data from October to March and hence limits the resolution of the full annual cycle. It highlights the need for more observations to better understand the transition between the winter and summer regimes.

By considering the seasonal variability, we have been able to explain previously reported inconsistencies in the current estimates [*Cuny et al*., 2002; *Myers et al*., 2007] and improve the overall transport numbers. Explicitly, we have shown that previous studies, which utilized only summer data, underestimate the property and velocity values by not resolving the seasonal cycle and hence, the annual mean values for the heat and volume transports. Freshwater transports, however, agree well with *Myers et al*. [2009] as they resolve the freshwater portion of the current well. In particular, our results indicate that studies that used only the summer data and restricted analysis to less than 700 m depth underestimate the mean IC temperature and volume transport by approximately 30%.

The decline in velocity of the boundary current from 1992 to 2008 is accompanied by a warming and salinity increase of the IC. The rates of change in the core of the IC are comparable to those of the interior and the density gradient remains approximately constant. This suggests that any changes in the volume transport are due to changes in the barotropic velocity. On the other hand, we found boundary current/interior anomalies in 1997 and 2003, associated with a rapid warming of the current and with its speeding up ("rapid" here refers to processes occurring on time scales on the order of a year). These changes propagate into the interior with a 2 year lag. This is supportive of the conclusion that anomalies propagating in the boundary current impact the interior. The implication is that changes in LSW properties and formation can result from advective anomalies that propagate into the region from upstream. This finding emphasizes the importance of the boundary current system and impacts our understanding of the heat and freshwater balances. The observed warming of the boundary current system over the last two decades is consistent with the previously reported trend in *Myers et al*. [2007]; however, their study was restricted to 700 m depth in vertical. Our results here resolve the full two-dimensional changes of the current both in width and depth space.

The observed slow-down of the surface circulation is consistent with the trend discussed by *Häkkinen and Rhines* [2004] and *Hakkinen and Rhines* [2009]. This change was initially attributed to reduced convective activity due to a decline in the buoyancy forcing. More recently, changes in the subpolar gyre have been

attributed to changes in ocean currents (partly tied to changes in wind stress) including anomalous intrusions of subtropical waters into the subpolar gyre [*Hátún et al*., 2005; *Häkkinen et al*., 2011]. Our results are consistent with this latter interpretation since we observe the propagation of anomalies from the boundary current to the interior. In terms of the slowdown, our study suggests that the slowdown is due to a decrease in the barotropic flow as opposed to a decrease in the baroclinic portion of the flow—since the interior/boundary current gradients we estimate did not show a trend.

Finally, an important result of this study is the documented rapid change in the boundary current properties and velocity of the boundary current in 1997 and 2003, which then propagated in the interior with a 2 year lag. Other studies have pointed to the uniqueness of these years. For example, *Lilly et al*. [2003] document an increase in the eddy activity in 1997 similarly to our study and suggest that prior to that year the eddies were present in the Labrador Sea in much smaller numbers. Our results suggest that the increase in eddies may be due to an increase in the baroclinicity of the boundary current in 1997 (and in 2003). The implication is that anomalies propagating around the subpolar gyre impact the Labrador Sea interior through changes in the lateral fluxes tied to eddy production [e.g., *Straneo et al*., 2013, and references therein]. This means that variations in LSW properties and formation rates are controlled not only by the surface fluxes but also by changes in boundary currents on interannual time scales.

Acknowledgments

T.R. and F.S. were supported by NSF OCE grants 0525929 and 0850416. A.B. was supported by NSF OCE grant 0623192. We thank Igor Yashayaev who generously allowed us to use Bedford Institution of Oceanography hydrographic data and the crew of all the cruises that collected the data. Hydrobase data are available at www.whoi.edu/science/PO/hydrobase/, and ICES hydrographic data are available at www.ices.dk. The altimeter products were produced by Ssalto/Duacs and distributed by Aviso with support from CNES (AVISO data can be accessed from www.aviso.oceanobs.com). We also gratefully acknowledge the feedback from Paul Myers and another anonymous reviewer who provided useful comments that improved the clarity and the content of the manuscript.

References

Ablain, M., A. Cazenave, G. Valladeau, and S. Guinehut (2009), A new assessment of the error budget of global mean sea level rate estimated by satellite altimetry over 1993–2008, *Ocean Sci.*, *5*(2), 193–201.

Avsic, T., J. Karstensen, U. Send, and J. Fischer (2006), Interannual variability of newly formed Labrador Sea water from 1994 to 2005, *Geophys. Res. Lett.*, *33*, L21S02, doi:10.1029/2006GL026913.

Bacon, S., P. G. Myers, B. Rudels, and D. A. Sutherland (2008), Accessing the inaccessible: Buoyancy-driven coastal currents on the shelves of Greenland and eastern Canada, in *Arctic-Subarctic Ocean Fluxes*, edicated by R. R. Dickson, J. Meincke and P. Rhines, pp. 703–722, Springer, Netherlands.

Bersch, M., I. Yashayaev, and K. P. Koltermann (2007), Recent changes of the thermohaline circulation in the subpolar North Atlantic, *Ocean Dyn.*, *57*(3), 223–235.

Böning, C. W., M. Scheinert, J. Dengg, A. Biastoch, and A. Funk (2006), Decadal variability of subpolar gyre transport and its reverberation in the North Atlantic overturning, *Geophys. Res. Lett.*, *33*, L21S01, doi:10.1029/2006GL026906.

Bower, A. S., M. S. Lozier, S. F. Gary, and C. W. Böning (2009), Interior pathways of the North Atlantic meridional overturning circulation, *Nature*, *459*(7244), 243–247.

Bracco, A., J. Pedlosky, and R. S. Pickart (2008), Eddy formation near the west coast of Greenland, *J. Phys. Oceanogr.*, *38*(9), 1992–2002.

Brandt, P., F. A. Schott, A. Funk, and C. S. Martins (2004), Seasonal to interannual variability of the eddy field in the Labrador Sea from satellite altimetry, *J. Geophys. Res.*, *109*, C02028, doi:10.1029/2002JC001551.

Cuny, J., P. B. Rhines, P. P. Niiler, and S. Bacon (2002), Labrador Sea boundary currents and the fate of the Irminger Sea water, *J. Phys. Oceanogr.*, *32*(2), 627–647.

Curry, R., and C. Mauritzen (2005), Dilution of the northern North Atlantic Ocean in recent decades, *Science*, *308*(5729), 1772–1774.

Daniault, N., H. Mercier, and P. Lherminier (2011), The 1992–2009 transport variability of the east Greenland-Irminger current at 60°N, *Geophys. Res. Lett.*, *38*, L07601, doi:10.1029/2011GL046863.

de Jong, M. F., A. S. Bower, and H. H. Furey (2014), Two years of observations of warm-core anticyclones in the Labrador Sea and their seasonal cycle in heat and salt stratification, *J. Phys. Oceanogr.*, *44*(2), 427–444.

de Steur, L., E. Hansen, R. Gerdes, M. Karcher, E. Fahrbach, and J. Holfort (2009), Freshwater fluxes in the East Greenland Current: A decade of observations, *Geophys. Res. Lett.*, *36*, L23611, doi:10.1029/2009GL041278.

Dickson, B., I. Yashayaev, J. Meincke, B. Turrell, S. Dye, and J. Holfort (2002), Rapid freshening of the deep north Atlantic Ocean over the past four decades, *Nature*, *416*(6883), 832–837.

Dickson, R. R., and J. Brown (1994), The production of north Atlantic deep water: Sources, rates, and pathways, *J. Geophys. Res.*, *99*(C6), 12,319–12,341.

Fratantoni, P. S., and R. S. Pickart (2007), The western North Atlantic shelfbreak current system in summer, *J. Phys. Oceanogr.*, *37*(10), 2509–2533.

Fu, L.-L., and A. Cazenave (2000), *Satellite Altimetry and Earth Sciences: A Handbook of Techniques and Applications*, vol. 69, Academic, San Diego, Calif.

Fu, L.-L., E. J. Christensen, C. A. Yamarone, M. Lefebvre, Y. Menard, M. Dorrer, and P. Escudier (1994), Topex/Poseidon mission overview, *J. Geophys. Res.*, *99*(C12), 24,369–24,381.

Häkkinen, S., and P. B. Rhines (2004), Decline of subpolar north Atlantic circulation during the 1990s, *Science*, *304*(5670), 555–559.

Hakkinen, S., and P. B. Rhines (2009), Shifting surface currents in the northern North Atlantic Ocean, *J. Geophys. Res.*, *114*, C04005, doi:10.1029/2008JC004883.

Häkkinen, S., P. B. Rhines, and D. L. Worthen (2011), Warm and saline events embedded in the meridional circulation of the northern north Atlantic, *J. Geophys. Res.*, *116*, C03006, doi:10.1029/2010JC006275.

Hall, M. M., D. J. Torres, and I. Yashayaev (2013), Absolute velocity along the AR7W section in the Labrador Sea, *Deep Sea Res., Part I*, *72*, 72–87.

Han, G., K. Ohashi, N. Chen, P. G. Myers, N. Nunes, and J. Fischer (2010), Decline and partial rebound of the Labrador current 1993–2004: Monitoring ocean currents from altimetric and conductivity-temperature-depth data, *J. Geophys. Res.*, *115*, C12012, doi:10.1029/2009JC006091.

Hátún, H., A. B. Sandø, H. Drange, B. Hansen, and H. Valdimarsson (2005), Influence of the Atlantic subpolar gyre on the thermohaline circulation, *Science*, *309*(5742), 1841–1844.

Helland-Hansen, B. (1934), The Sognefjord section, in *James Johnstone Memorial Volume*, vol. 348, pp. 257–274, Univ. Press of Liverpool.
Holliday, N., S. Bacon, J. Allen, and E. McDonagh (2009), Circulation and transport in the western boundary currents at cape farewell, Greenland, *J. Phys. Oceanogr.*, *39*(8), 1854–1870.
Hurrell, J. W., Y. Kushnir, and M. Visbeck (2001), The North Atlantic oscillation, *Science*, *291*(5504), 603–605.
Katsman, C. A., M. A. Spall, and R. S. Pickart (2004), Boundary current eddies and their role in the restratification of the Labrador Sea, *J. Phys. Oceanogr.*, *34*(9), 1967–1983.
Kwok, R. (2004), Annual cycles of multiyear sea ice coverage of the Arctic Ocean: 1999–2003, *J. Geophys. Res.*, *109*, C11004, doi:10.1029/2003JC002238.
Lab Sea Group (1998), The Labrador Sea deep convection experiment, *Bull. Am. Meteorol. Soc.*, *79*(10), 2033–2058.
Lavender, K. L., R. E. Davis, and W. B. Owens (2002), Observations of open-ocean deep convection in the Labrador Sea from subsurface floats, *J. Phys. Oceanogr.*, *32*(2), 511–526.
Lazier, J., R. Hendry, A. Clarke, I. Yashayaev, and P. Rhines (2002), Convection and restratification in the Labrador Sea, 1990–2000, *Deep Sea Res., Part I*, *49*(10), 1819–1835.
Lilly, J. M., P. B. Rhines, F. Schott, K. Lavender, J. Lazier, U. Send, and E. DAsaro (2003), Observations of the Labrador Sea eddy field, *Prog. Oceanogr.*, *59*(1), 75–176.
Marshall, J., and F. Schott (1999), Open-ocean convection: Observations, theory, and models, *Rev. Geophys.*, *37*(1), 1–64.
Myers, P. G., N. Kulan, and M. H. Ribergaard (2007), Irminger water variability in the west Greenland current, *Geophys. Res. Lett.*, *34*, L17601, doi:10.1029/2007GL030419.
Myers, P. G., C. Donnelly, and M. H. Ribergaard (2009), Structure and variability of the west Greenland current in summer derived from 6 repeat standard sections, *Prog. Oceanogr.*, *80*(1), 93–112.
Pickart, R. (2013), Adventure in the Labrador Sea, *Life*, *50*(2). [Available at http://www.whoi.edu/oceanus/feature/adventure-in-the-labrador-sea.]
Pickart, R. S., and M. A. Spall (2007), Impact of Labrador Sea convection on the north Atlantic meridional overturning circulation, *J. Phys. Oceanogr.*, *37*(9), 2207–2227.
Pickart, R. S., D. J. Torres, and R. Clarke (2002), Hydrography of the Labrador Sea during active convection, *J. Phys. Oceanogr.*, *32*(2), 428–457.
Prater, M. D. (2002), Eddies in the Labrador Sea as observed by profiling rafos floats and remote sensing, *J. Phys. Oceanogr.*, *32*(2), 411–427.
Rhein, M., J. Fischer, W. Smethie, D. Smythe-Wright, R. Weiss, C. Mertens, D.-H. Min, U. Fleischmann, and A. Putzka (2002), Labrador Sea water: Pathways, cfc inventory, and formation rates, *J. Phys. Oceanogr.*, *32*(2), 648–665.
Rykova, T., F. Straneo, J. M. Lilly, and I. Yashayaev (2009), Irminger current anticyclones in the Labrador Sea observed in the hydrographic record, 1990–2004, *J. Mar. Res.*, *67*, 361–384, doi:10.1357/002224009789954739.
Rykova, T. A. (2010), The seasonal and interannual variability of the west Greenland current system in the Labrador Sea, PhD thesis, Massachusetts Inst. Technol., Cambridge, U. K.
Sarafanov, A., H. Mercier, A. Falina, A. Sokov, and P. Lherminier (2010), Cessation and partial reversal of deep water freshening in the northern north Atlantic: Observation-based estimates and attribution, *Tellus, Ser. A*, *62*(1), 80–90.
Schmidt, S., and U. Send (2007), Origin and composition of seasonal Labrador Sea freshwater, *J. Phys. Oceanogr.*, *37*(6), 1445–1454.
Smith, W., and D. Sandwell (1997), Global sea floor topography from satellite altimetry and ship depth soundings, *Science*, *277*(5334), 1956–1962.
Spall, M. A. (2004), Boundary currents and watermass transformation in marginal seas, *J. Phys. Oceanogr.*, *34*(5), 1197–1213.
Stein, M. (2005), North Atlantic subpolar gyre warming—Impacts on Greenland offshore waters, *J. Northwest Atl. Fish. Sci.*, *36*, 43–54.
Straneo, F. (2006a), Heat and freshwater transport through the central Labrador Sea, *J. Phys. Oceanogr.*, *36*(4), 606–628.
Straneo, F. (2006b), On the connection between dense water formation, overturning, and poleward heat transport in a convective basin, *J. Phys. Oceanogr.*, *36*(9), 1822–1840.
Straneo, F., G. S. Hamilton, D. A. Sutherland, L. A. Stearns, F. Davidson, M. O. Hammill, G. B. Stenson, and A. Rosing-Asvid (2010), Rapid circulation of warm subtropical waters in a major glacial fjord in east Greenland, *Nat. Geosci.*, *3*(3), 182–186.
Straneo, F., et al. (2013), Challenges to understanding the dynamic response of Greenland's marine terminating glaciers to oceanic and atmospheric forcing, *Bull. Am. Meteorol. Soc.*, *94*(8), 1131–1144.
Våge, K., et al. (2011), The Irminger gyre: Circulation, convection, and interannual variability, *Deep Sea Res., Part I*, *58*(5), 590–614.
Yashayaev, I., H. M. van Aken, N. P. Holliday, and M. Bersch (2007), Transformation of the Labrador Sea water in the subpolar North Atlantic, *Geophys. Res. Lett.*, *34*, L22605, doi:10.1029/2007GL031812.